Numerical Methods for an Oil Recovery Model

Jackson Sweeney
Supervisor: Jérôme Droniou
Monash University

Contents

1 Introduction

The Peaceman model describes an oil extraction process by which a solvent is injected into a reservoir via a well so as to force the oil out via a second well. The model is a coupled system of partial differential equations (PDEs) with three unknowns: the pressure of the mixture, $p(\mathbf{x}, t)$, the Darcy velocity $\mathbf{u}(\mathbf{x}, t)$ of the mixture, and the concentration of the injected solvent $c(\mathbf{x}, t)$. Note that the concentration is a quantity between 0 and 1 which describes the fraction of injected solvent in the fluid mixture.

Let Ω be a bounded domain in $\mathbf{R}^2$ and [0,T] be an interval in time. We denote the permeability tensor and the porosity of the medium by $\mathbf{K}(\mathbf{x})$ and $\phi(\mathbf{x})$ respectively, while $\mu(c)$ denotes the viscosity of the fluid mixture. Neglecting gravity, the Peaceman model is given by:

$$\begin{aligned} \nabla\cdot\mathbf{u} &= q^+ - q^- \qquad (\mathbf{x}, t) \in \Omega \times [0, T], \\ \mathbf{u} &= -\frac{\mathbf{K}}{\mu(c)}\nabla p \qquad (\mathbf{x}, t) \in \Omega \times [0, T], \end{aligned} \tag{1.0.1}$$

$$\phi\frac{\partial c}{\partial t} + \nabla \cdot (\mathbf{u}c - \mathbf{D}(\mathbf{x}, \mathbf{u})\nabla c) = \bar{c}q^+ - cq^- \qquad (\mathbf{x}, t) \in \Omega \times [0, T], \tag{1.0.2}$$

where q^+ and q^- represent the injection and production wells respectively, $\bar{c}$ is the concentration of injected fluid, and $\mathbf{D}(\mathbf{x}, \mathbf{u})$ denotes the diffusion-dispersion tensor:

$$\mathbf{D}(\mathbf{x}, \mathbf{u}) = \phi(\mathbf{x})\left[d_m\mathbf{I} + \frac{d_l}{|\mathbf{u}|}\begin{pmatrix} u_x^2 & u_xu_y \\ u_xu_y & u_y^2 \end{pmatrix} + \frac{d_t}{|\mathbf{u}|}\begin{pmatrix} u_y^2 & -u_xu_y \\ -u_xu_y & u_x^2 \end{pmatrix}\right], \tag{1.0.3}$$

where d_m is the molecular diffusion coefficient, while d_l and d_t are the longitudinal and transverse dispersion coefficients respectively. Note that u_x and u_y refer to the x and y components of the Darcy velocity respectively. Further, notice that the second and third terms in the above expression are simply the projection matrices in the directions $\mathbf{u}$ and $\mathbf{u}^\perp$ respectively, weighted by coefficients ϕd_l and ϕd_t.

We impose the following *no-flow* boundary conditions, which ensure that no fluid leaves or enters the reservoir except via the injection and production wells:

$$\begin{aligned} \mathbf{u}\cdot\mathbf{n} &= 0, \ (\mathbf{x}, t) \in \partial\Omega \times [0, T], \\ (\mathbf{D}\nabla c)\cdot\mathbf{n} &= 0, \ (\mathbf{x}, t) \in \partial\Omega \times [0, T]. \end{aligned} \tag{1.0.4}$$

Additionally, we impose the following condition on the injection and production wells:

$$\int_\Omega (q^+ - q^-)\ d\mathbf{x} = 0. \tag{1.0.5}$$

This ensures that the total mass of fluid in the reservoir remains constant.

Mathematically, these wells are typically represented as delta functions:

$$\begin{aligned} q^+ &= r\delta(\mathbf{x} - \mathbf{x}^+), \\ q^- &= r\delta(\mathbf{x} - \mathbf{x}^-), \end{aligned} \tag{1.0.6}$$

where $\mathbf{x}^+$ and $\mathbf{x}^-$ are the locations of the injection and production wells respectively, and r is the flow rate of fluid through the wells.

It is necessary to specify an initial condition for the concentration:

$$c(\mathbf{x}, 0) = c_0(\mathbf{x}),\ \mathbf{x} \in \Omega. \tag{1.0.7}$$

We note that the above only specifies the pressure up to an additive constant. We therefore impose the following condition on p:

$$\int_\Omega p(\mathbf{x}, t)\ d\mathbf{x} = 0,\ t \in [0, T]. \tag{1.0.8}$$

2 A Primer on Finite Element Methods (FEMs)

In this section we introduce the basic concepts involved in finite element methods by way of a simple example. We refer the reader to, for example, Johnson [2009] for a more comprehensive introduction.

Suppose we wish to solve the following boundary value problem (BVP)

$$\begin{aligned} -\nabla \cdot (\mathbf{A}\nabla u) &= f \qquad \mathbf{x} \in \Omega, \\ \nabla u \cdot \mathbf{n} &= 0 \qquad \mathbf{x} \in \partial\Omega, \end{aligned} \tag{2.0.9}$$

where Ω is a bounded domain in $\mathbf{R}^2$, $\mathbf{A}$ is a 2×2 matrix and $\mathbf{n}$ is the outward pointing normal on $\partial\Omega$. We now introduce the inner product space

$$\begin{aligned} V = \{&v : v \text{ is continuous on } \Omega,\ v = 0 \text{ on } \partial\Omega, \text{ and all partial derivatives of } v \\ &\text{are continuous and bounded on } \Omega\}, \end{aligned}$$

with inner product

$$(u, v) = \int_\Omega uv \; d\mathbf{x}. \tag{2.0.10}$$

We also define

$$a(u, v) = \int_\Omega \mathbf{A}\nabla u \cdot \nabla v \; d\mathbf{x}. \tag{2.0.11}$$

We note that every solution u of (2.0.9) is an element of V. Then it may be shown that (2.0.9) is formally equivalent to the following statement

$$a(u, v) = (f, v) \qquad \forall v \in V, \tag{2.0.12}$$

where we have obtained (2.0.12) by multiplying the first equation in (2.0.9) by v, an arbitrary element of V called a *test function*, and integrating over Ω.

At this point, it must be noted that V is an infinite dimensional space. The essential idea of the finite element method is that we in some sense substitute V with a finite dimensional subspace, say V_h. The finite element method consists in finding $u_h \in V_h$ such that

$$a(u_h, v_h) = (f, v_h) \qquad \forall v_h \in V_h. \tag{2.0.13}$$

Note that throughout this report, we will use the subscript h to denote a finite element counterpart to a particular variable or function.

We construct such a subspace V_h as follows: we first choose a finite set of points $T = \{\mathbf{x}_1, \mathbf{x}_2, \ldots, \mathbf{x}_m\}$ in Ω. We then choose a family of functions such that any member of this family may be uniquely determined by its values at each of the aforementioned finite set of points, T. We call the points in T *degrees of freedom*. We may then construct a basis for V_h, $\{z_i\}$, such that

$$z_i(x_j) = \begin{cases} 1 \text{ if } i = j \\ 0 \text{ if } i \neq j \end{cases} \tag{2.0.14}$$

For any $j \in 1, 2..., m$, the following special case of (2.0.13) holds

$$a(u_h, z_j) = (f, z_j). \tag{2.0.15}$$

We then write u_h as a weighted sum of basis functions

$$u_h = \sum_{i=1}^{n} b_i z_i. \tag{2.0.16}$$

Combining (2.0.15) and (2.0.16) we obtain

$$\sum_{i=1}^{n} b_i a(u_h, z_j) = (f, z_j), \tag{2.0.17}$$

which is a system of m linear equations with m unknowns $\{a_1, a_2, ..., a_m\}$. Solving for these m unknowns we may then construct our approximate solution to (2.0.9), u_h, from the basis functions $\{z_i\}$.

3 FEMs for the Peaceman Model

3.1 Overview

In this section we present two similar, but subtly different finite element schemes for solving the Peaceman model approximately. These methods are due to Ewing et al. [1983] and Wang et al. [2000] respectively. Both methods utilise a *mixed finite element method* (MFEM) to solve (1.0.1). This is presented in section 3.2. (1.0.2) is more complex as it involves both a convection term and a diffusion term. The convection term in particular requires some care; many simple methods for handling convection result in unstable oscillatory solutions. In this report we focus on *characteristic methods* as a means of handling the convection term. These are methods in which particles are tracked along specific curves known as *characteristics*. This is discussed in section 3.3. Ewing et al. [1983] uses what we call the *modified method of characteristics*, or MMOC, while Wang et al. [2000] uses an *Eulerian-Lagrangian localised adjoint method*, or ELLAM. Following this, we present both methods in full in sections 3.3.1 and 3.3.2 respectively.

Much of the following is derived from Wang et al. [2000] and to a lesser extent Ewing et al. [1983], though we have modified some of Wang's notation and simplified much of the overall presentation.

3.2 The Pressure Equation: Mixed Finite Element Methods

Mixed finite element methods are a simple, although not trivial, extension of standard finite elements to cases involving more than one independent variable. In particular, these methods are often used in cases with one independent variable, but where, for instance, the derivative of that independent variable is of most interest.

We now recall the relevant portion of the problem statement in the introduction:

$$\begin{aligned} \nabla \cdot \mathbf{u} &= q^+ - q^- \text{ in } \Omega,\ t \in [0,T], \\ \mathbf{u} &= -\frac{\mathbf{K}}{\mu(c)} \nabla p \text{ in } \Omega,\ t \in [0,T], \\ \mathbf{u} \cdot \mathbf{n} &= 0 \text{ on } \partial\Omega,\ t \in [0,T], \\ \int_\Omega p\ d\mathbf{x} &= 0,\ t \in [0,T]. \end{aligned} \tag{3.2.1}$$

Let $L^2(\Omega)$ be the space of Lebesgue square integrable functions on Ω, that is

$$L^2(\Omega) = \left\{ f \middle| \left(\int_\Omega |f(\mathbf{x})|^2 d\mathbf{x} \right)^{\frac{1}{2}} < \infty \right\}. \tag{3.2.2}$$

Then define

$$\begin{aligned} L_0^2(\Omega) &= \left\{ v \in L^2(\Omega) \middle| \int_\Omega v(\mathbf{x}) d\mathbf{x} = 0 \right\}, \\ H(div;\Omega) &= \left\{ \mathbf{v} \in (L^2(\Omega))^2 \middle| \nabla \cdot \mathbf{v} \in L^2(\Omega) \right\}, \\ H_0(div;\Omega) &= \left\{ \mathbf{v} \in H(div;\Omega) \middle| \mathbf{v}(\mathbf{x}) \cdot \mathbf{n} = 0, \quad \mathbf{x} \in \partial\Omega \right\}. \end{aligned} \tag{3.2.3}$$

Note that $p \in L_0^2$ and $\mathbf{u} \in H_0(div;\Omega)$. Let $w \in L_0^2$ and $\mathbf{v} \in H_0(div;\Omega)$. We now multiply the first equation in (3.2.1) by w and the second equation in (3.2.1) by $\mathbf{v}$, integrating both over Ω. Note that we have also multiplied the second equation by $\mu(c)\mathbf{K}^{-1}$.

$$\begin{aligned} \int_\Omega w \nabla \cdot \mathbf{u}\ d\mathbf{x} &= \int_\Omega (q^+ - q^-) w\ d\mathbf{x}, \\ \int_\Omega \mu(c)\mathbf{K}^{-1}\mathbf{u} \cdot \mathbf{v}\ d\mathbf{x} &= -\int_\Omega \nabla p \cdot \mathbf{v}\ d\mathbf{x}, \\ &\forall \mathbf{v} \in H_0(div;\Omega), \qquad \forall w \in L_0^2(\Omega). \end{aligned} \tag{3.2.4}$$

We now restrict these spaces L_0^2 and $H_0(div;\Omega)$ to finite dimensional subspaces, as in the section 2.

For simplicity, suppose that Ω is a rectangular domain in $\mathbf{R}^2$, say $(x_{min}, x_{max}) \times (y_{min}, y_{max})$. We then define the following space-time partition:

$$\begin{aligned} x_{min} = x_0^p < x_1^p <...< x_{P-1}^p < x_P^p = x_{max}, \\ y_{min} = y_0^p < y_1^p <...< y_{Q-1}^p < y_Q^p = y_{max}, \\ 0 = t_0^p < t_1^p <...< t_{M-1}^p < t_M^p = T. \end{aligned} \tag{3.2.5}$$

We use this to define a rectangular mesh of cells with vertices given by (x_i^p, y_j^p), $i \in 1, 2, ..., P$, $j \in 1, 2, ..., Q$.

We then define

$$\begin{aligned} W_0^p(\Omega) &= \left\{ w \,\middle|\, w \text{ is constant in each cell, } \int_\Omega w(\mathbf{x}) d\mathbf{x} = 0 \right\}, \\ M_x^p(\Omega) &= \left\{ f \,\middle|\, f \text{ is continuous in } x,\ f \text{ is piecewise constant in } y, \right. \\ &\qquad \left. f\,(x,y) = (ax+b) \text{ on each cell, } f(x_{min}, \cdot) = f(x_{max}, \cdot) = 0 \right\}, \\ M_y^p(\Omega) &= \left\{ g \,\middle|\, g \text{ is continuous in } y,\ g \text{ is piecewise constant in } x \right. \\ &\qquad \left. g\,(x,y) = (cy+d) \text{ on each cell, } g(\cdot, y_{min}) = g(\cdot, y_{max}) = 0 \right\}, \\ S_0^p(\Omega) &= \left\{ \mathbf{v} \,\middle|\, \mathbf{v}(\mathbf{x}) = (f(x,y), g(x,y)),\ f(x,y) \in M_x^p(\Omega), g(x,y) \in M_y^p(\Omega) \right\}. \end{aligned} \tag{3.2.6}$$

We use W_0^p as our finite dimensional subspace of L_0^2, and S_0^p as our finite dimensional subspace of $H_0(div; \Omega)$. Note that there are several other possible choices of subspace for this kind of method, although a complete discussion of the advantages and disadvantages of these choices is beyond the scope of this report. We note however that this choice of S_0^p allows the boundary condition $\mathbf{u}_h \cdot \mathbf{n} = 0$ to be satisfied exactly, where $\mathbf{u}_h \in S_0^p$ is the numerical Darcy velocity.

This MFEM consists in finding $p_h \in W_0^p$ and $\mathbf{u}_h \in S_0^p$ such that

$$\begin{aligned} \int_\Omega w_h \nabla \cdot \mathbf{u}_h(\mathbf{x}, t_m^p)\ d\mathbf{x} &= \int_\Omega (q^+ - q^-) w_h\ d\mathbf{x}, \\ \int_\Omega \mu(c_h(\mathbf{x}, t_m^p))\mathbf{K}^{-1}\mathbf{u}_h(\mathbf{x}, t_m^p) \cdot \mathbf{v}_h\ d\mathbf{x} &= \int_\Omega p_h(\mathbf{x}, t_m^p) \nabla \cdot \mathbf{v}_h\ d\mathbf{x}, \\ \forall \mathbf{v}_h \in S_0^p(\Omega), \qquad & \forall w_h \in W_0^p(\Omega). \end{aligned} \tag{3.2.7}$$

As in section 2, we solve this by constructing bases for $S_0^p(\Omega)$ and $W_0^p(\Omega)$ from a set of degrees of freedom. This in turn allows us to construct a system of linear equations, whose solution yields $p_h(\mathbf{x}, t_m^p)$ and $\mathbf{u}_h(\mathbf{x}, t_m^p)$.

3.3 The Concentration Equation: Characteristic Methods

We recall the relevant information from the problem statement in the introduction:

$$\begin{aligned} \phi \frac{\partial c}{\partial t} + \nabla \cdot (\mathbf{u}c - \mathbf{D}(\mathbf{x}, \mathbf{u}) \nabla c) = \bar{c} q^+ - c q^- \qquad & (\mathbf{x}, t) \in \Omega \times [0, T], \\ (\mathbf{D} \nabla c) \cdot \mathbf{n} = 0 \qquad & (\mathbf{x}, t) \in \partial\Omega \times [0, T]. \end{aligned} \tag{3.3.1}$$

We again define a spacetime partition, assuming for simplicity that Ω is rectangular:

$$\begin{aligned} x_{min} = x_0^c < x_1^c < ... < x_{I-1}^c < x_I^c = x_{max}, \\ y_{min} = y_0^c < y_1^c < ... < y_{J-1}^c < y_J^c = y_{max}, \\ 0 = t_0^c < t_1^c < ... < t_{N-1}^c < t_N^c = T, \end{aligned} \tag{3.3.2}$$

again defining a rectangular mesh of cells with vertices given by (x_i^c, y_j^c), $i \in 1, 2, ..., I$, $j \in 1, 2, ..., J$. We let $\Delta t_n^c = t_n^c - t_{n-1}^c$.

We then define the following finite dimensional space of piecewise bilinear functions, which will be used to generate test functions for both the MMOC and ELLAM methods.

$$\begin{aligned} S^c(\Omega) = \Big\{ z \Big| & z \text{ is continuous on } \Omega, \text{ and in each cell} \\ & z(x, y) = a_{00} + a_{10}x + a_{01}y + a_{11}xy \Big\}. \end{aligned} \tag{3.3.3}$$

Note that any $z \in S^c(\Omega)$ may be completely determined from its values at the vertices of the rectangular mesh defined in (3.3.2).

3.3.1 The Modified Method of Characteristics (MMOC)

We modify the first equation in (3.3.1) by applying the following vector identity

$$\nabla \cdot (\mathbf{u}c) = \mathbf{u} \cdot \nabla c + c\nabla \cdot \mathbf{u}. \tag{3.3.4}$$

We recall from the introduction that $\nabla \cdot \mathbf{u} = q^+ - q^-$. Hence, we obtain

$$\phi \frac{\partial c}{\partial t} + \mathbf{u} \cdot \nabla c - \nabla \cdot (\mathbf{D}\nabla c) = (\bar{c} - c)q^+ \qquad (\mathbf{x}, t) \in \Omega \times [0, T]. \tag{3.3.5}$$

We refer to this as a *non-conservative* form of the concentration equation. By contrast, the first equation in (3.3.1) is a *conservative* form.

We integrate over $\Omega \times [t^c_{n-1}, t^c_n]$ against test functions $z(\mathbf{x}) \in S^c(\Omega)$ and substitute the exact $\mathbf{u}$ and c with the approximate $\mathbf{u}_h$ and c_h.

We then define the following characteristic curves $\mathbf{r}(t)$

$$\frac{d\mathbf{r}(t)}{dt} = \frac{\mathbf{u}_h(\mathbf{r}(t), t)}{\phi(\mathbf{r}(t))}. \tag{3.3.6}$$

If we differentiate the numerical concentration along these curves, we find that

$$\phi \frac{dc_h(\mathbf{r}(t), t)}{dt} = \phi(\mathbf{r}(t)) \frac{\partial c_h(\mathbf{r}(t), t)}{\partial t} + \mathbf{u}_h(\mathbf{r}(t), t) \cdot \nabla c_h(\mathbf{r}(t), t). \tag{3.3.7}$$

We may then make the following approximation:

$$\phi(\mathbf{x}) \frac{\partial c_h(\mathbf{x}, t^c_n)}{\partial t} + \mathbf{u}_h(\mathbf{x}, t^c_n) \cdot \nabla c_h(\mathbf{x}, t^c_n) \approx \phi(\mathbf{x}) \frac{c_h(\mathbf{x}, t^c_n) - c_h(\mathbf{x}^*, t^c_{n-1})}{\Delta t^c_n}. \tag{3.3.8}$$

where $\mathbf{x} = \mathbf{r}(t^c_n)$ and $\mathbf{x}^* = \mathbf{r}(t^c_{n-1})$ may be found as follows

$$\mathbf{x}^* = \mathbf{x} - \int_{t^c_{n-1}}^{t^c_n} \frac{\mathbf{u}_h(\mathbf{x}, t)}{\phi(\mathbf{x})} dt. \tag{3.3.9}$$

In Ewing et al. [1983], an approximate characteristic tracking is used; $\mathbf{x}^*$ is approximated by the following equation

$$\mathbf{x}^* = \mathbf{x} - \Delta t^c_n \frac{\mathbf{u}_h(\mathbf{x}, t^c_n)}{\phi(\mathbf{x})}. \tag{3.3.10}$$

However, an approximate tracking is in general not necessary, since the form of $\mathbf{u}_h$, given in (3.2.6), is simple and can be integrated analytically. Since $\mathbf{u}_h$ satisfies the no-flow boundary condition $\mathbf{u}_h \cdot \mathbf{n} = 0$ exactly, this ensures that the point $\mathbf{x}^*$ will always remain inside the domain.

With this in mind, after some manipulation we arrive at the following scheme: find $c_h(\mathbf{x}, t_n^c) \in S^c(\Omega)$ such that

$$\begin{aligned}
&\int_\Omega \phi(\mathbf{x}) c_h(\mathbf{x}, t_n^c) z_h(\mathbf{x}) d\mathbf{x} + \Delta t_n^c \int_\Omega \nabla z_h(\mathbf{x}) \cdot \mathbf{D}(\mathbf{x}, \mathbf{u}_h(\mathbf{x}, t_n^c)) \nabla c_h(\mathbf{x}, t_n^c) d\mathbf{x} \\
&= \int_\Omega \phi(\mathbf{x}) c_h(\mathbf{x}^*, t_{n-1}^c) z_h(\mathbf{x}) d\mathbf{x} + \Delta t_n^c \int_\Omega (\bar{c} - c_h(\mathbf{x}, t_n^c)) q^+ z_h(\mathbf{x}) d\mathbf{x}, \\
&\qquad \forall z_h \in S^c(\Omega). \qquad (3.3.11)
\end{aligned}$$

3.3.2 The Eulerian-Lagrangian Localised Adjoint Method (ELLAM)

In contrast with the MMOC presented in the previous section, the ELLAM scheme consists in multiplying the conservative form of the concentration equation given in (3.3.1) by suitable test functions z and integrating over $\Omega \times [t_{n-1}^c, t_n^c]$, and replacing the concentration and test functions c and z by their finite element counterparts c_h and z_h. Unlike the MMOC, the ELLAM requires that the test functions z_h be time-dependent. We must therefore extend the purely spatial test functions used previously over the time interval $[t_{n-1}^c, t_n^c]$. Given this, and after some manipulation, in particular applying the boundary condition in (3.3.1) and applying the product rule to the term involving $\frac{\partial c_h}{\partial t}$, we find the following:

$$\begin{aligned}
&\int_{t_{n-1}^c}^{t_n^c} \int_\Omega \phi(\mathbf{x}) \frac{\partial (c_h(\mathbf{x}, t) z_h(\mathbf{x}, t))}{\partial t} d\mathbf{x} dt \\
&+ \int_{t_{n-1}^c}^{t_n^c} \int_\Omega \nabla z_h(\mathbf{x}, t) \cdot \mathbf{D}(\mathbf{x}, \mathbf{u}_h(\mathbf{x}, t)) \nabla c_h(\mathbf{x}, t) d\mathbf{x} dt \\
&- \int_{t_{n-1}^c}^{t_n^c} \int_\Omega c_h(\mathbf{x}, t) \left[\phi(\mathbf{x}) \frac{\partial z_h(\mathbf{x}, t)}{\partial t} + \mathbf{u}_h(\mathbf{x}, t) \cdot \nabla z_h(\mathbf{x}, t) \right] d\mathbf{x} dt \qquad (3.3.12) \\
&= \int_{t_{n-1}^c}^{t_n^c} \int_\Omega (\bar{c} q^+ - c_h(\mathbf{x}, t) q^-) z_h(\mathbf{x}, t) d\mathbf{x} dt.
\end{aligned}$$

We specify the test functions z_h to be elements of the following space:

$$\begin{aligned}
S^{c,e}(\Omega \times [t_{n-1}^c, t_n^c]) = \Bigg\{ z_h \Bigg| & z_h(\mathbf{x}, t_n^c) \in S^c(\Omega),\ \phi(\mathbf{x}) \tfrac{\partial z_h(\mathbf{x}, t)}{\partial t} + \mathbf{u}_h(\mathbf{x}, t) \cdot \nabla z_h(\mathbf{x}, t) = 0 \\
& \forall (\mathbf{x}, t) \in \Omega \times [t_{n-1}^c, t_n^c] \Bigg\}. \qquad (3.3.13)
\end{aligned}$$

In essence, what we have done here is choose our test functions to be constant on the characteristic curves defined in (3.3.6).

We then obtain the following scheme: find $c_h(\mathbf{x}, t_n^c) \in S^c(\Omega)$ such that

$$\begin{aligned}
&\int_\Omega \phi(\mathbf{x}) c_h(\mathbf{x}, t_n^c) z_h(\mathbf{x}, t_n^c) d\mathbf{x} + \Delta t_n^c \int_\Omega \nabla z_h(\mathbf{x}, t_n^c) \cdot \mathbf{D}(\mathbf{x}, \mathbf{u}_h(\mathbf{x}, t_n^c)) \nabla c_h(\mathbf{x}, t_n^c) d\mathbf{x} \\
&= \int_\Omega \phi(\mathbf{x}) c_h(\mathbf{x}, t_{n-1}^c) z_h(\mathbf{x}, t_{n-1}^{c,+}) d\mathbf{x} + \Delta t_n^c \int_\Omega (\bar{c} q^+ - c_h(\mathbf{x}, t_n^c) q^-) z_h(\mathbf{x}) d\mathbf{x}, \\
&\quad \forall z_h \in S^{c,e}(\Omega \times [t_{n-1}^c, t_n^c]).
\end{aligned} \tag{3.3.14}$$

The test functions z_h are discontinuous in time at each t_n^c. When approximating the partial derivative in the first integral of (3.3.12) we use the limit of z_h as t approaches t_{n-1}^c from above, which we denote by $z_h(\mathbf{x}, t_{n-1}^{c,+})$. In practice, this is evaluated by forward tracking the point $\mathbf{x}$ along the characteristic curves to find

$$\mathbf{x}^{**} = \mathbf{x} + \int_{t_{n-1}^c}^{t_n^c} \frac{\mathbf{u}_h(\mathbf{x}, t_n^c)}{\phi(\mathbf{x})} d\mathbf{x}. \tag{3.3.15}$$

and then using the fact that the test functions are constant on the characteristics, so

$$z_h(\mathbf{x}, t_{n-1}^{c,+}) = z_h(\mathbf{x}^{**}, t_n^c). \tag{3.3.16}$$

An important property of the ELLAM scheme is that it conserves mass. This can be shown by rewriting (3.3.14) setting the test functions z_h equal to 1 everywhere.

$$\begin{aligned}
\int_\Omega \phi(\mathbf{x}) c_h(\mathbf{x}, t_n^c) d\mathbf{x} = &\int_\Omega \phi(\mathbf{x}) c_h(\mathbf{x}, t_{n-1}^c) d\mathbf{x} \\
&+ \Delta t_n^c \int_\Omega (\bar{c} q^+ - c_h(\mathbf{x}, t_n^c) q^-) d\mathbf{x}.
\end{aligned} \tag{3.3.17}$$

In plainer terms, this states that the change in mass of solvent in the reservoir over a given timestep is exactly equal to the mass of solvent injected or removed via the two wells during that timestep. Conversely, if we perform the same analysis to the MMOC, we find

$$\begin{aligned}
\int_\Omega \phi(\mathbf{x}) c_h(\mathbf{x}, t_n^c) d\mathbf{x} = &\int_\Omega \phi(\mathbf{x}) c_h(\mathbf{x}^*, t_{n-1}^c) d\mathbf{x} \\
&+ \Delta t_n^c \int_\Omega (\bar{c} - c_h(\mathbf{x}, t_n^c)) q^+ d\mathbf{x}.
\end{aligned} \tag{3.3.18}$$

This implies that the MMOC violates conservation of mass. This represents a significant disadvantage of the MMOC when compared with the ELLAM.

3.3.3 A Note on Characteristic Tracking

One of the differences between the ELLAM and MMOC methods is that they use forward and backward tracking schemes respectively. In practice, these tracking schemes are more or less the same - the only difference is the direction of integration along the characteristic curves.

The tracking algorithm employed in these schemes is due to Russell and Trujillo [1990]. The integration is carried out on a cell-by-cell basis; the velocity $\frac{\mathbf{u}_h}{\phi}$ has the form $(ax+b, cy+d)$ where the coefficients a, b, c, d are constant on each cell. A typical point will usually be tracked through multiple cells over the course of one timestep. In our implementation, we approach this problem using what Schafer-Perini and Wilson [1991] refer to as the *mixed distance and time method* - a given point is tracked until it reaches a cell boundary, at which point the coefficients a, b, c, d for the new cell are retrieved and the process repeated until the point has been tracked over a full timestep. This is done for several points in each cell so that the relevant integrals in the ELLAM and MMOC schemes may be evaluated numerically.

3.4 An MFEM-MMOC scheme

When combining the MFEM and MMOC schemes to solve the full Peaceman model, there are several additional considerations we must address. We first note that typically in these kinds of simulations, the concentration changes much more rapidly than either the Darcy velocity or the pressure. It is therefore often computationally advantageous to use coarser time and spatial steps for the evaluation of the pressure equation. A consequence of this is that we may perform several iterations on the concentration equation for each iteration on the pressure equation without significantly altering the numerical solution. We therefore define integers

$$0 = N_0 < N_1 < ... < N_m < ... < N_{M-1} < N_M = N, \tag{3.4.1}$$

where

$$t^c_{N_m} = t^p_m. \tag{3.4.2}$$

The coupling of the two equations presents an additional difficulty. Solving the concentration equation at time t^c_n requires the Darcy velocity at t^c_n, while solving the

pressure equation at t_m^p requires the concentration at t_m^p. It is therefore necessary to define an approximation to the Darcy velocity via extrapolation from previous timesteps:

$$(E\mathbf{u}_h)(\mathbf{x}, t_n^c) = \left(1 + \frac{t_n^c - t_{m-1}^p}{t_{m-1}^p - t_{m-2}^p}\right)\mathbf{u}_h(\mathbf{x}, t_{m-1}^p) - \frac{t_n^c - t_{m-1}^p}{t_{m-1}^p - t_{m-2}^p}\mathbf{u}_h(\mathbf{x}, t_{m-2}^p),$$
$$n = N_{m-1}+1, N_{m-1}+2, ..., N_m, \quad m = 2, 3, ..., M,$$
$$(E\mathbf{u}_h)(\mathbf{x}, t_n^c) = \mathbf{u}_h(\mathbf{x}, 0), \quad n = 1, 2, ..., N_1, \quad m = 1. \tag{3.4.3}$$

We now present the full MFEM-MMOC scheme:

for $m = 0$, $n = 0$

Step 1. Project the initial condition $c_0(\mathbf{x})$ onto the space $S^c(\Omega)$. That is, find $c_h(\mathbf{x}, 0) \in S^c(\Omega)$ such that

$$\int_\Omega c_h(\mathbf{x}, 0) z_h(\mathbf{x}) d\mathbf{x} = \int_\Omega c_0(\mathbf{x}) z_h(\mathbf{x}) d\mathbf{x}, \qquad \forall z_h(\mathbf{x}) \in S^c(\Omega). \tag{3.4.4}$$

Step 2. Solve the MFEM given in (3.2.7) at t = 0. Find $p_h(\mathbf{x}, 0) \in W_0^p$ and $\mathbf{u}_h(\mathbf{x}, 0) \in S_0^p$ such that

$$\begin{aligned} \int_\Omega w_h \nabla \cdot \mathbf{u}_h(\mathbf{x}, 0)\ d\mathbf{x} &= \int_\Omega (q^+ - q^-) w_h\ d\mathbf{x}, \\ \int_\Omega \mu(c_h(\mathbf{x}, 0))\mathbf{K}^{-1}\mathbf{u}_h(\mathbf{x}, 0) \cdot \mathbf{v}_h\ d\mathbf{x} &= \int_\Omega p_h(\mathbf{x}, 0) \nabla \cdot \mathbf{v}_h\ d\mathbf{x}, \\ & \forall \mathbf{v}_h \in S_0^p(\Omega), \qquad \forall w_h \in W_0^p(\Omega). \end{aligned} \tag{3.4.5}$$

end

for $m = 1, 2, ..., M$

Step 3.

for $n = N_{m-1} + 1, n = N_{m-1} + 2, ..., N_m$

Solve the MMOC scheme given in (3.3.11) using the Darcy velocity extrapolation $E\mathbf{u}_h$. That is, find $c(\mathbf{x}, t_n^c) \in S^c(\Omega)$ such that

$$\begin{aligned} &\int_\Omega \phi(\mathbf{x}) c_h(\mathbf{x}, t_n^c) z_h(\mathbf{x}) d\mathbf{x} + \Delta t_n^c \int_\Omega \nabla z_h(\mathbf{x}) \cdot \mathbf{D}(\mathbf{x}, (E\mathbf{u}_h)(\mathbf{x}, t_n^c)) \nabla c_h(\mathbf{x}, t_n^c) d\mathbf{x} \\ &= \int_\Omega \phi(\mathbf{x}) c_h(\mathbf{x}^*, t_{n-1}^c) z_h(\mathbf{x}) d\mathbf{x} + \Delta t_n^c \int_\Omega (\bar{c} - c_h(\mathbf{x}, t_n^c)) q^+ z_h(\mathbf{x}) d\mathbf{x}, \\ &\qquad \forall z_h \in S^c(\Omega). \end{aligned} \tag{3.4.6}$$

end

Step 4. Using the fact that $t^c_{N_m} = t^p_m$, use the concentration from the final iteration of the previous step to solve the MFEM system given in (3.2.7) at time t^p_m. Find $p_h(\mathbf{x}, t^p_m) \in W^p_0$ and $\mathbf{u}_h(\mathbf{x}, t^p_m) \in S^p_0$ such that

$$\begin{aligned} \int_\Omega w_h \nabla \cdot \mathbf{u}_h(\mathbf{x}, t^p_m)\ d\mathbf{x} &= \int_\Omega (q^+ - q^-) w_h\ d\mathbf{x}, \\ \int_\Omega \mu(c_h(\mathbf{x}, t^p_m))\mathbf{K}^{-1}\mathbf{u}_h(\mathbf{x}, t^p_m) \cdot \mathbf{v}_h\ d\mathbf{x} &= \int_\Omega p_h(\mathbf{x}, t^p_m) \nabla \cdot \mathbf{v}_h\ d\mathbf{x}, \qquad (3.4.7) \\ & \forall \mathbf{v}_h \in S^p_0(\Omega), \qquad \forall w_h \in W^p_0(\Omega). \end{aligned}$$

end

3.5 An MFEM-ELLAM scheme

The MFEM-ELLAM scheme is identical to the MFEM-MMOC scheme except that step 3 is replaced by the following:

for $n = N_{m-1} + 1, n = N_{m-1} + 2, ..., N_m$

Solve the ELLAM scheme given in (3.3.14) using the Darcy velocity extrapolation $E\mathbf{u}_h$. That is, find $c(\mathbf{x}, t^c_n) \in S^c(\Omega)$ such that

$$\begin{aligned} &\int_\Omega \phi(\mathbf{x}) c_h(\mathbf{x}, t^c_n) z_h(\mathbf{x}, t^c_n) d\mathbf{x} + \Delta t^c_n \int_\Omega \nabla z_h(\mathbf{x}, t^c_n) \cdot \mathbf{D}(\mathbf{x}, (E\mathbf{u}_h)(\mathbf{x}, t^c_n)) \nabla c_h(\mathbf{x}, t^c_n) d\mathbf{x} \\ &= \int_\Omega \phi(\mathbf{x}) c_h(\mathbf{x}, t^c_{n-1}) z_h(\mathbf{x}, t^{c,+}_{n-1}) d\mathbf{x} + \Delta t^c_n \int_\Omega (\bar{c} q^+ - c_h(\mathbf{x}, t^c_n) q^-) z_h(\mathbf{x}) d\mathbf{x}, \\ &\quad \forall z_h \in S^{c,e}(\Omega \times [t^c_{n-1}, t^c_n]). \qquad (3.5.1) \end{aligned}$$

end

4 Numerical Results

In this section, we present the results of a series of tests of both the MFEM-ELLAM and MFEM-MMOC methods. The following parameters are common to all of our tests, except where noted:

- A rectangular domain, $\Omega = (0, 1000) \times (0, 1000)$ ft^2.
- An injection well located at (1000,1000) with flow rate 30 ft^2/day.
- A production well located at (0,0) with flow rate 30 ft^2/day.
- A constant porosity $\phi = 0.1$.
- An injection concentration of $\bar{c} = 1$.
- An oil viscosity of $\mu(0) = 1.0$ cp.
- A uniform spatial grid with spacing $\Delta x^c = \Delta y^c = \Delta x^p = \Delta y^p = 50$ ft.
- A timestep of $\Delta t^p = \Delta t^c = 360$ days.
- An initial condition $c(\mathbf{x}, 0) = 0$.

4.1 The MFEM-ELLAM scheme

Test 1. To test the MFEM-ELLAM scheme, we use a permeability of $\mathbf{K} = 80\mathbf{I}$, where $\mathbf{I}$ is the 2x2 identity tensor. Further, we specify a mobility ratio $M = 1$, molecular diffusion $\phi d_m = 1.0$ ft^2/day, longitudinal dispersion $\phi d_l = 0.0$ ft and transverse dispersion $\phi d_t = 0.0$ ft. The results of this test are shown in Figure 4.1.1.

These results are highly problematic. The exact solution of the Peaceman model under these conditions is bounded above by 1, so we expect the numerical solution to be, at the very least, bounded above by some number slightly larger than 1. This numerical solution however explodes to well above 50 at the injection well. In fact, this explosion can be made arbitrarily large by varying the amount of fluid injected into the reservoir per unit time. Moreover this explosion occurs after one timestep - this is significant since it rules out the convection term as a source of the issue. If we refer to equation (3.3.14), we notice that for the first timestep, the first term on the left hand side - the convection term - is zero. The source of the explosion must therefore be either the diffusion term or the well terms. We examine this more closely in subsequent tests.

We must note that this concentration explosion at the injection well is not present in the results shown in Wang et al. [2000]. It is our opinion that the issue almost certainly lies with Wang et al. [2000] rather than with our results, since we were able to confirm our results at t = 1 year with two near-independent codes. To elaborate, we first constructed a code using MATLAB which produced the results shown in Figure

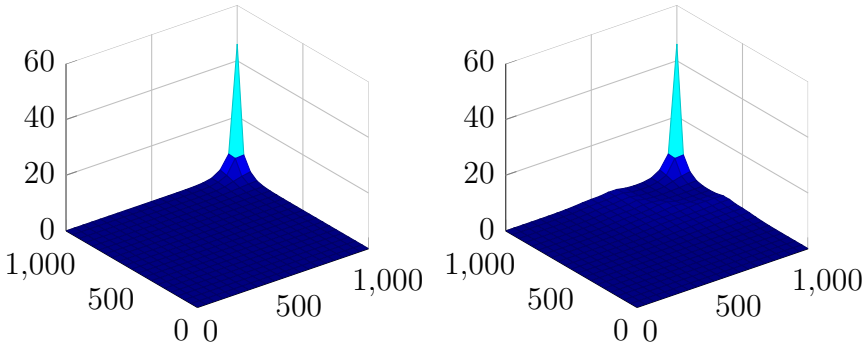

Figure 4.1.1: The concentration of the invading fluid for the ELLAM scheme in test 1 at $t = 1$ year (left) and $t = 3$ years (right)

4.1.1. We then discovered a second code written in C++ for a similar ELLAM scheme, published online in Liu [2009]. This code deals only with the concentration equation and so can only readily be used to simululate one timestep of the method we wish to study. Furthermore, it was necessary to modify slightly this code in order that it be applicable to the Peaceman model. Nevertheless, with these very small modifications the C++ code produced identical results to those shown in the left panel of Figure 4.1.1. This should, at the very least, raise some strong doubt as to the veracity of the results presented in Wang et al. [2000].

Test 2. To identify the source of the issue, we test the MFEM-ELLAM scheme with diffusion, but no convection, injection or production terms. That is, we set $q^+ = q^- = 0$ and use a non-zero initial condition $c(x, y, 0) = \sin(\frac{\pi x}{1000}) \sin(\frac{\pi y}{1000})$. We again set $\phi d_m = 1.0$ ft^2/day, $\phi d_l = 0.0$ ft and $\phi d_t = 0.0$ ft. The results of this test are shown in Figure 4.1.2.

This test shows quite conclusively that the issue is not with the diffusion term - the behaviour seen here is exactly what one would expect from the solution to a diffusion equation. In particular, notice that for large values of t, the solution is very close to a constant function equal to the mean of the initial condition.

Test 3. To test the convection term we again set $q^+ = q^- = 0$, but use a Darcy velocity which is constant with $u_x = u_y = 0.02$ on $(50, 950) \times (50, 950)$ and on the remainder of Ω is such that it is an element of the space $S_0^p(\Omega)$ defined in (3.2.6). For the purposes of this test however, we will be considering a solution which is close to zero near the boundary, so we can consider the Darcy velocity essentially constant.

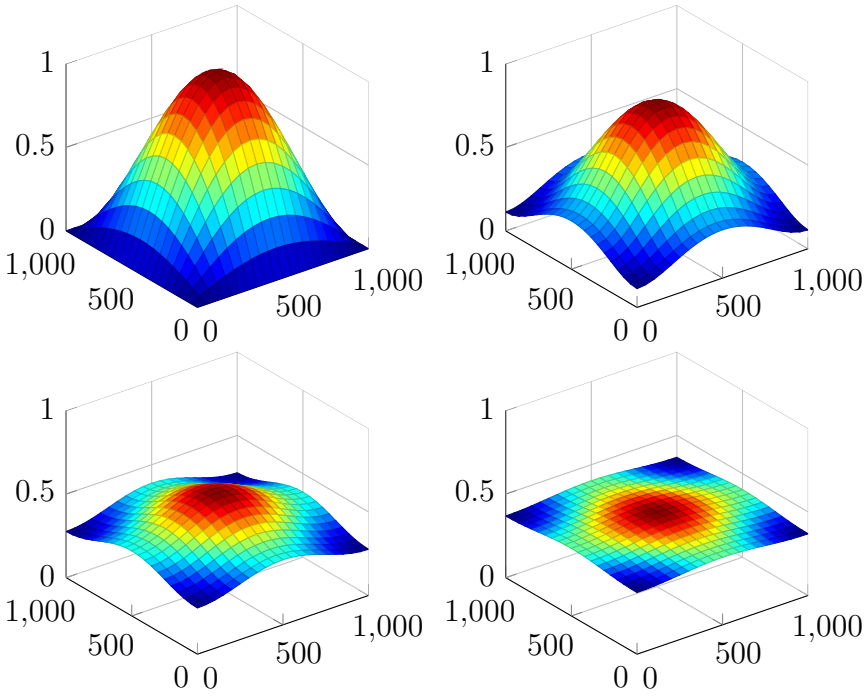

Figure 4.1.2: The concentration for the ELLAM scheme in test 2 at $t = 0$ years (top left), $t = 3$ years (top right), $t = 10$ years (bottom left) and $t = 20$ years (bottom right)

We take a non-zero initial condition

$$c(x, y, 0) = \begin{cases} \sin(\frac{\pi(x-100)}{600}) \sin(\frac{\pi(y-100)}{600}) & \text{on } (100, 700) \times (100, 700), \\ 0 & \text{elsewhere.} \end{cases} \tag{4.1.1}$$

To eliminate diffusion, we set $\phi d_m = 0.0$ ft^2/day, $\phi d_l = 0.0$ ft and $\phi d_t = 0.0$ ft. We are essentially solving a pure advection equation

$$\phi \frac{\partial c}{\partial t} + \nabla \cdot (c\mathbf{u}) = 0. \tag{4.1.2}$$

The results, shown in Figure 4.1.3, are again as expected; the sinusoidal pulse is advected with constant speed. The issue is therefore not with the implementation of the method of characteristics. This confirms the deduction we made from the fact that

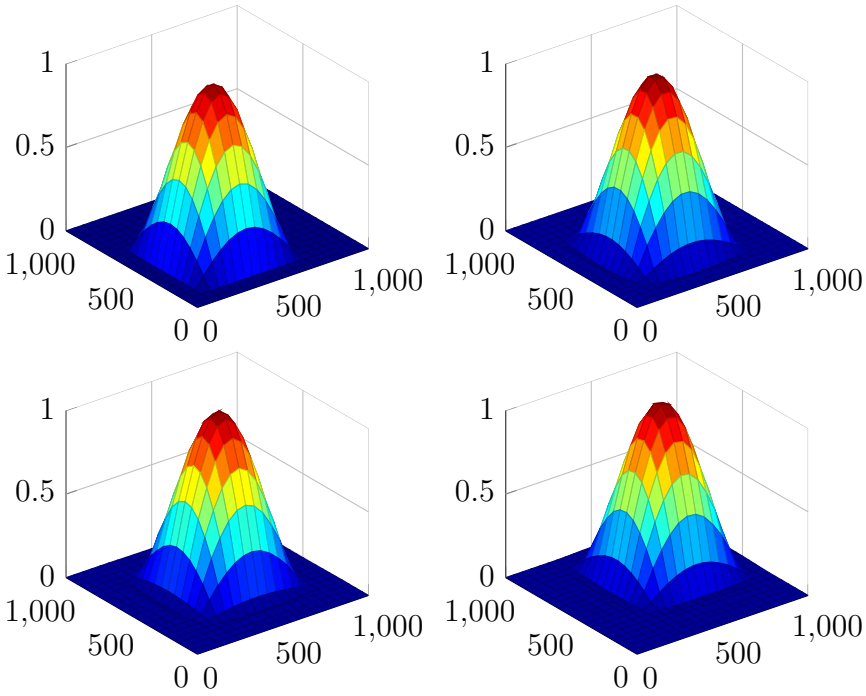

Figure 4.1.3: The concentration for the ELLAM scheme in test 3 at $t = 0$ year (top left), $t = 1$ years (top right), $t = 2$ years (bottom left) and $t = 3$ years (bottom right)

the concentration explosion appears after one timestep in test 1, and moreover shows that the ELLAM handles convection quite well.

Test 4. We use the same parameters as in test 3, but add a source term. In particular, we choose q^+ and q^- to satisfy the pressure $\nabla \cdot \mathbf{u} = q^+ - q^-$. To do this we let $q = \nabla \cdot \mathbf{u}$ and let q^+ and q^- be the positive and negative parts of q respectively. We note that here q is positive for $x < 50$ and for $y < 50$. The results of this test are shown in Figure 4.1.4.

The results again show an explosion in the injection region after one timestep, so we conclude that the source of the issue with the ELLAM scheme is the injection term.

Test 5. We now wish to test to see if the results produced by the MFEM-ELLAM method improve under different conditions. We use the same $\mathbf{K}$, M, ϕd_m, ϕd_t and ϕd_l as in test 1, but use a much smaller timestep $\Delta t^c = 18$ days. Additionally, we use injection and production wells spread over four cells rather than using delta functions. This has the effect of significantly reducing the spike in concentration over the injection

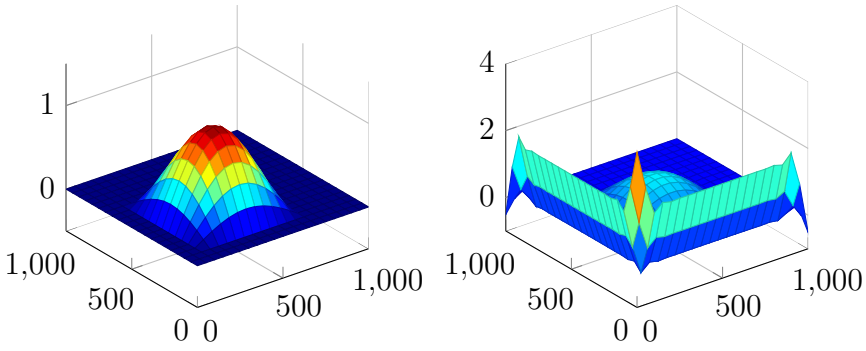

Figure 4.1.4: The concentration for the ELLAM scheme in test 4 at $t = 0$ years (left) and $t = 1$ year (right)

region. The results are shown in Figure 4.1.5.

These results show a drastic improvement over test 1; there are still some abnormalities in the injection region, but they are substantially reduced in size when compared with previous tests. Moreover, the solution behaves more or less as expected throughout the rest of the domain, and is in fact similar to the results shown in Wang et al. [2000] under the conditions used in test 1. This suggests that the MFEM-ELLAM scheme may still converge to the exact solution as the timestep approaches zero. A formal convergence analysis is however needed to confirm this.

4.2 The MFEM-MMOC scheme

For the most part, the parameters used in these tests will follow those used in Droniou and Chanais-Hillairet [2007], in which a mixed finite volume method is tested. The results of this method will serve as a point of comparison for the MFEM-MMOC scheme.

Test 1. We use the same conditions as in test 1 for the MFEM-ELLAM scheme. The results are shown in Figure 4.2.1.

These results are more or less exactly what we expect from this kind of scheme. Indeed, these results agree very well not only with the results presented in Wang et al. [2000] and Ewing et al. [1983], but also with the results of other methods, for example the mixed finite volume scheme used in Droniou and Chanais-Hillairet [2007]. In particular, we note that at $t = 3$ years the concentration contours form a family of concentric circles. This is physically reasonable since the viscosity μ and the permeability $\mathbf{K}$ are constant, resulting in a radial Darcy velocity $\mathbf{u}$. We also note

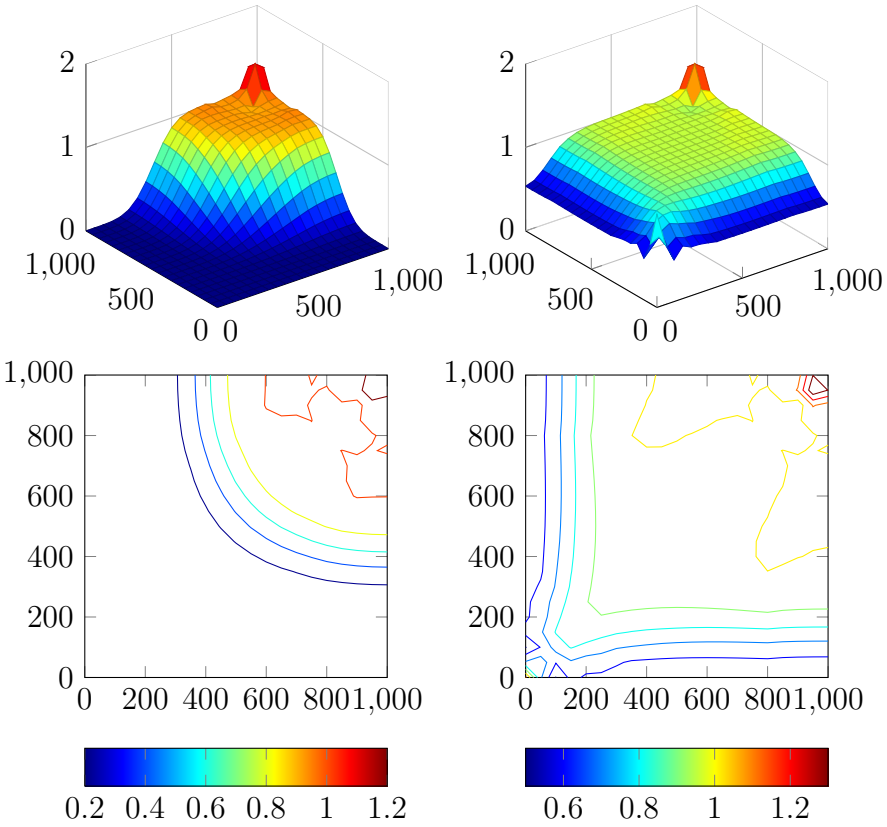

Figure 4.1.5: The concentration for the ELLAM scheme in test 5 at $t = 3$ years (left) and $t = 10$ years (right)

that at $t = 10$ years the fluid seems to be moving faster along the diagonal joining the injection and production wells. This is again physically reasonable since the fluid can only exit the reservoir via the production well.

Test 2. We again use constant permeability $\mathbf{K} = 80\mathbf{I}$, but use a mobility ratio of $M = 41$ and a diffusion-dispersion tensor specified by $\phi d_m = 0.0$, $\phi d_l = 5.0$ and $\phi d_t = 0.5$. These conditions are more realistic than those used in test 1 - practically speaking dispersion dominates diffusion in this kind of porous medium flow, so it is reasonable to set molecular diffusion to zero.

The results of this test again compare well with those presented in Droniou and Chanais-Hillairet [2007]. In particular, we note that the high mobility ratio of 41 causes the transition from $c = 0$ to $c = 1$ to be much sharper than in the previous tests. Furthermore, the fluid moves much faster along the diagonal than in test 1 due

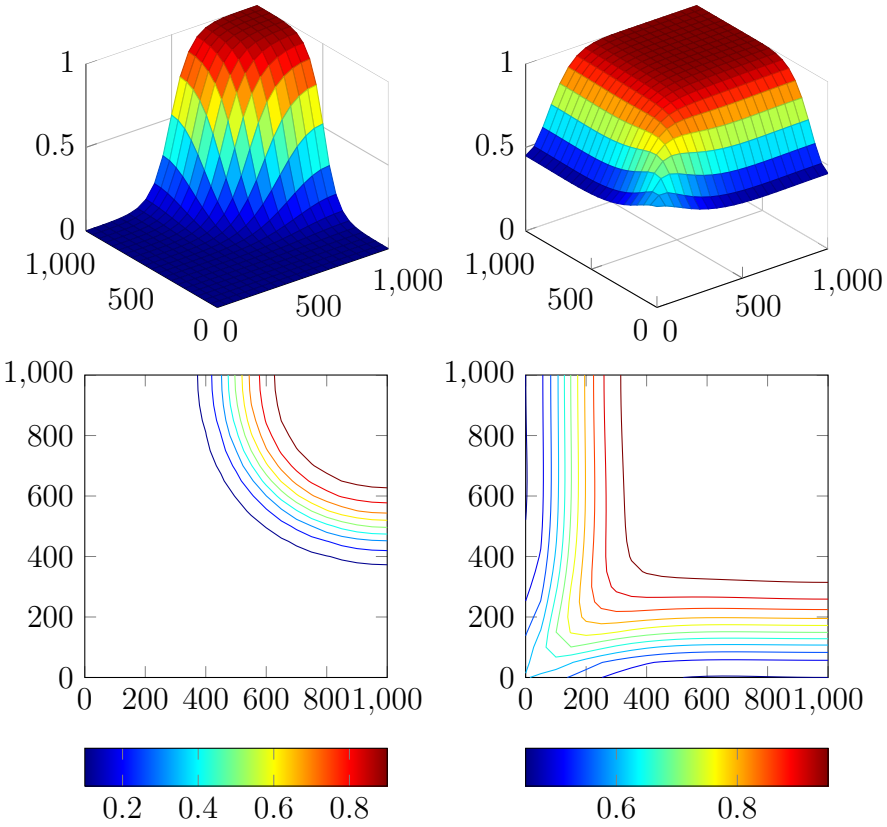

Figure 4.2.1: The concentration for the MMOC scheme in test 1 at $t = 3$ years (left) and $t = 10$ years (right)

to the large difference between the longitudinal and transverse dispersivities.

We do however note two key differences between these results and those presented in Droniou and Chanais-Hillairet [2007]. Firstly, the mixed finite volume scheme employed in Droniou and Chanais-Hillairet [2007] produces substantial *numerical diffusion* - spurious diffusion effects due to the solution method rather than the Peaceman model itself. This numerical diffusion is not present in the results of the MFEM-MMOC scheme. In particular, we note that the transition from $c = 0$ to $c = 1$ is much sharper in these results than in the results of the mixed finite volume scheme.

Secondly, we refer to the left panel of Figure 4.2.3, which shows a cross section at $x = 400$ of the surface plot at $t = 10$ years from Figure 4.2.2. What this shows is that the MFEM-MMOC method tends to overshoot $c = 1$ and undershoot $c = 0$ at sharp fluid interfaces. The mixed finite volume method used in Droniou and Chanais-Hillairet

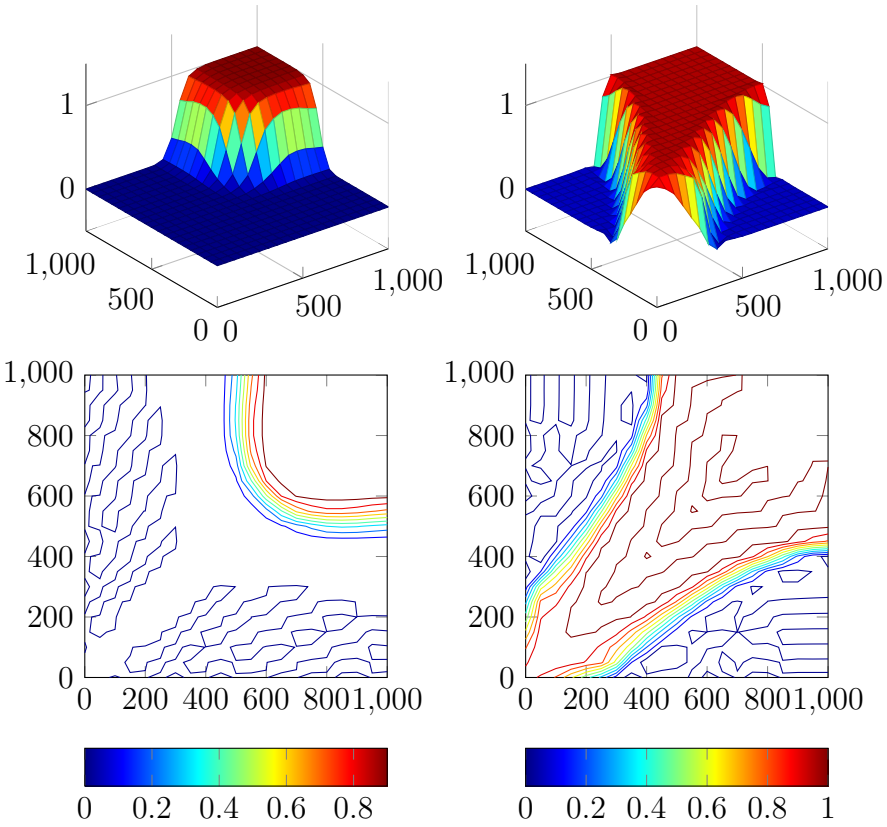

Figure 4.2.2: The concentration for the MMOC scheme in test 2 at $t = 3$ years (left) and $t = 10$ years (right)

[2007] avoids this problem entirely. A related problem with the MFEM-MMOC method is that it produces many small oscillations in regions where the concentration should be near-constant. This is clearly visible in the contour plot shown in Figure 4.2.2. We do note however that the overshoot present in the MFEM-MMOC results is substantially reduced with a refined spatial grid, as shown in the right panel of Figure 4.2.3.

Test 3. We use the same conditions as in test 2, with the exception that we take a discontinuous permeability tensor $\mathbf{K}(\mathbf{x})$ equal to $80\mathbf{I}$ on $(0, 1000) \times (0, 500)$, and equal to $20\mathbf{I}$ on $(0, 1000) \times (500, 1000)$. The results of this test are shown in Figure 4.2.4.

The lower permeability on $(0, 1000) \times (500, 1000)$ means that the Darcy velocity is much smaller there than on $(0, 1000) \times (0, 500)$. The fluid therefore initially moves very slowly, but suddenly increases in speed once it reaches the boundary between the two subdomains, $y = 500$. These results again agree very well with those presented in

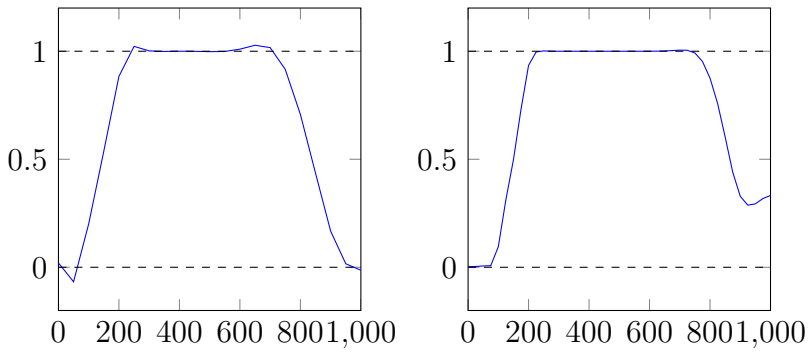

Figure 4.2.3: A cross section of the results of the MMOC scheme in test 2 at $x = 400$ ft after $t = 10$ years. The left panel shows this with $\Delta x = \Delta y = 50$ ft, while the right panel uses a refined grid with $\Delta x = \Delta y = 25$ ft

Droniou and Chanais-Hillairet [2007].

Test 4. We again use the same conditions as in test 2 with a discontinuous permeability tensor. Here we take $\mathbf{K}(\mathbf{x})$ equal to $20\mathbf{I}$ on the subdomains $(200, 400) \times (200, 400)$, $(200, 400) \times (600, 800)$, $(600, 800) \times (200, 400)$ and $(600, 800) \times (600, 800)$, and equal to $80\mathbf{I}$ elsewhere in Ω. The results are shown in Figure 4.2.5.

Again these results are physically reasonable and qualitatively agree with those produced by other methods. However, we note that there are substantial problems with overshoot on the subdomains where $\mathbf{K} = 20\mathbf{I}$. In particular, at $t = 15$ years we note that the concentration spikes to around -0.48 at $(250, 250)$. Eliminating these spikes entirely requires a much finer spatial grid on each of these subdomains where $\mathbf{K} = 20\mathbf{I}$. We also note that this negative spike is not present in the results produced by the mixed finite volume scheme in Droniou and Chanais-Hillairet [2007]. This represents a significant advantage of the mixed finite volume method over the MMOC.

5 Conclusion

Our results show that the MFEM-MMOC scheme due to Ewing et al. [1983], modified to use exact characteristic tracking, produces physically reasonable results even when using very large timesteps. We note that this method produces very little numerical diffusion, but has issues with overshoot at sharp fluid interfaces. Conversely, the MFEM-ELLAM scheme due to Wang et al. [2000] produces very poor results which do not agree with those presented in the aforementioned paper. We note that this scheme

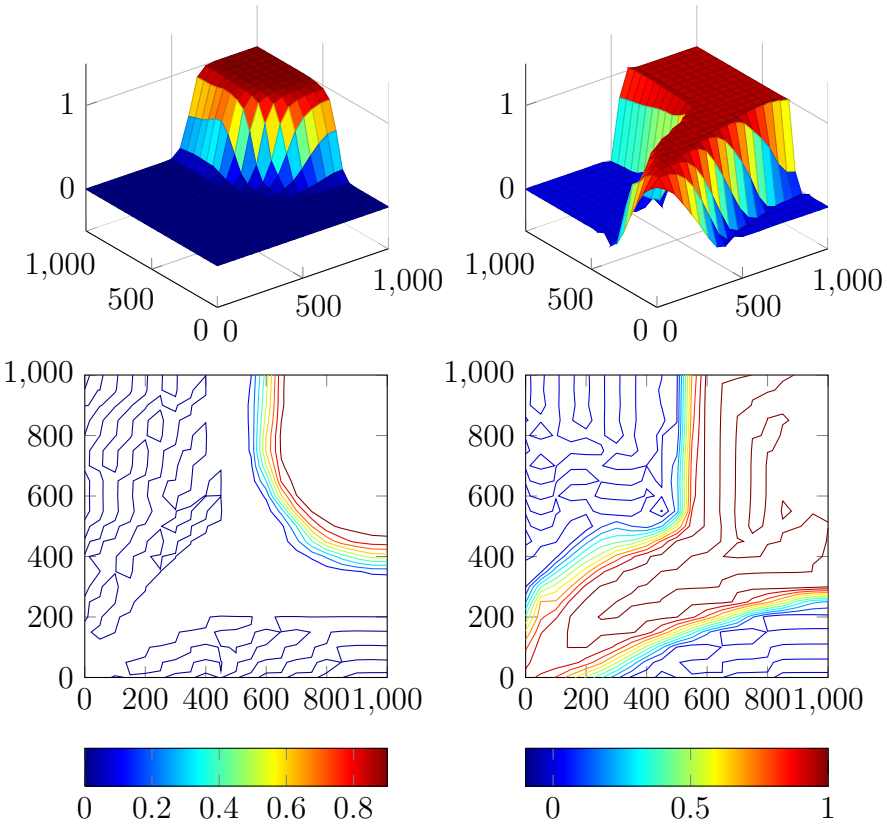

Figure 4.2.4: The concentration for the MMOC scheme in test 3 at $t = 3$ years (left) and $t = 10$ years (right)

handles convection and diffusion very well, but has significant issues in the handling of source terms. Since we were unable to reproduce the results presented in Wang et al. [2000], we are forced to question their veracity.

5.1 Future work

One of the original aims of this project was ultimately to try to implement an ELLAM scheme in the context of the mixed finite volume method presented in Droniou and Chanais-Hillairet [2007]. The hope was that this would mitigate the numerical diffusion produced by said method. As the ELLAM method does not produce sensible results in a finite element context, this no longer seems like a practical path to follow. However, one possibility for future work is to try to implement a MMOC scheme in a mixed finite

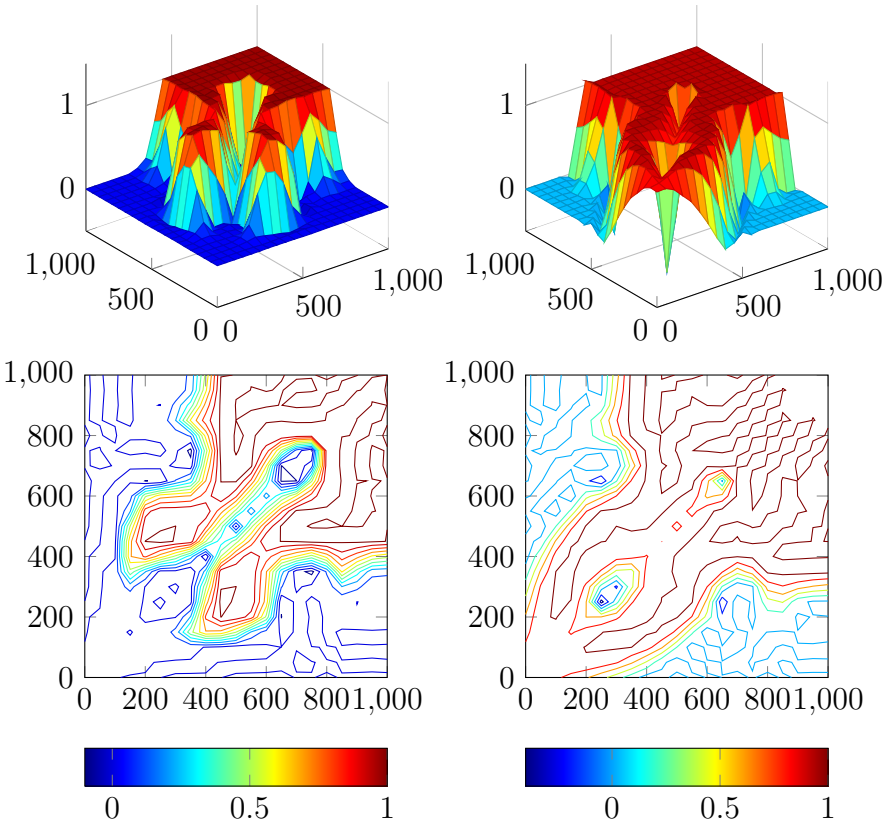

Figure 4.2.5: The concentration for the MMOC scheme in test 4 at $t = 5$ years (left) and $t = 15$ years (right)

volume context. This turns out to be difficult to do since the numerical Darcy velocity used in the mixed finite volume method is piecewise constant - it does not satisfy the no-flow boundary condition exactly. Characteristic tracking is therefore difficult as it is likely that points will be tracked out of the domain. Nonetheless, finding a way to circumvent this difficulty may be a potential object of future research.

We should also note that this present study of the MFEM-ELLAM scheme is incomplete. It may perhaps be worth investigating whether the ELLAM can be modified in some way so that it can better handle source terms. This may be particularly valuable if it can be done in a way that does not violate conservation of mass - this would give a potential modified ELLAM scheme an advantage over the MMOC. It would also be worth further investigating the convergence properties of the ELLAM to better understand why it produces such poor results.

6 Acknowledgements

Firstly, I would like to thank my supervisor Dr. Jérôme Droniou for his invaluable guidance and support. I would also like to thank Jérôme's PhD student Kyle Talbot for supplying me with a number of useful resources over the course of the project. Finally, I must of course thank Monash University and the AMSI for giving me this fantastic opportunity.

References

J. Droniou and C. Chanais-Hillairet. Convergence analysis of a mixed finite volume scheme for an elliptic-parabolic system modeling miscible fluid flows in porous media. *SIAM Journal of Numerical Analysis*, 45(5):2228–2258, 2007.

R. E. Ewing, T. F. Russell, and M. F. Wheeler. Simulation of miscible displacement using mixed methods and a modified method of characteristics. In *SPE Annual Conference Proceedings*, pages 71–81, 1983. SPE 12241.

C. Johnson. *Numerical Solution of Partial Differential Equations by the Finite Element Method*. Dover, New York, 2nd edition edition, 2009.

J. Liu. The white paper on ellam implementation in c++, 2009. URL `http://www.math.colostate.edu/~liu/ELLAM2d/ellam2d.pdf`. Accessed 18/2/2014.

T. F. Russell and R. V. Trujillo. Eulerian-lagrangian localized adjoint methods with variable coefficients in multiple dimensions. In *Computational Methods in Surface Hydrology, Proceedings of the 8th International conference on Computational Methods in Water Resources*, pages 357–363, 1990.

A. L. Schafer-Perini and J. L. Wilson. Efficient and accurate front tracking for two-dimensional groundwater flow models. *Water Resources Research*, 27:1471–1485, 1991.

H. Wang, D. Liang, R. E. Ewing, S. L. Lyons, and G. Qin. An approximation to miscible fluid flows in porous media with point sources and sinks by an eulerian-lagrangian localised adjoint method and mixed finite element methods. *SIAM Journal on Scientific Computing*, 22(2):561–581, 2000.